

# Diameter Modulation of Vertically Aligned Single-Walled Carbon Nanotubes

Rong Xiang<sup>1\*</sup>, Erik Einarsson,<sup>2,3</sup> Yoichi Murakami<sup>4</sup>, Junichiro Shiomi<sup>2</sup>, Shohei Chiashi<sup>2</sup>, Zikang Tang<sup>1,5</sup>,  
Shigeo Maruyama<sup>2\*</sup>

<sup>1</sup> State Key Laboratory of Optoelectronic Materials and Technologies, School of Physics and Engineering, Sun Yat-Sen University, Guangzhou 510275, China

<sup>2</sup> Department of Mechanical Engineering, The University of Tokyo, 7-3-1 Hongo, Bunkyo-ku, Tokyo 113-8656, Japan

<sup>3</sup> Global Center of Excellence for Mechanical Systems Innovation, The University of Tokyo, 7-3-1 Hongo, Bunkyo-ku, Tokyo 113-8656, Japan

<sup>4</sup> Global Edge Institute, Tokyo Institute of Technology, 2-12-1 Ookayama, Meguro-ku, Tokyo 152-8550, Japan

<sup>5</sup> Department of Physics, Hong Kong University of Science and Technology, Clear Water Bay, Hong Kong, China

---

\* To whom correspondence should be addressed.

Rong Xiang, [xiangr2@mail.sysu.edu.cn](mailto:xiangr2@mail.sysu.edu.cn), State Key Laboratory of Optoelectronic Materials and Technologies, School of Physics and Engineering, Sun Yat-Sen University, Guangzhou 510275, China;  
tel: +86-20-39943409; fax: +86-20-39943262

Shigeo Maruyama, [maruyama@photon.t.u-tokyo.ac.jp](mailto:maruyama@photon.t.u-tokyo.ac.jp), Department of Mechanical Engineering, The University of Tokyo, 7-3-1 Hongo, Bunkyo-ku, Tokyo 113-8656, Japan;  
tel: +81-3-5841-6421; fax: +81-3-5800-6983.

1  
2  
3 ABSTRACT  
4

5 We demonstrate wide-range diameter modulation of vertically aligned single-walled carbon  
6 nanotubes (SWNTs) using a wet chemistry prepared catalyst. In order to ensure compatibility to  
7  
8 electronic applications, the current minimum mean diameter of 2 nm for vertically aligned  
9  
10 SWNTs is challenged. The mean diameter is decreased to about 1.4 nm by reducing Co catalyst  
11  
12 concentrations to 1/100 or by increasing Mo catalyst concentrations by five times. We also  
13  
14 propose a novel spectral analysis method that allows one to distinguish absorbance contributions  
15  
16 from the upper, middle, and lower parts of a nanotube array. We use this method to  
17  
18 quantitatively characterize the slight diameter change observed along the array height. Based on  
19  
20 further investigation of the array and catalyst particles, we conclude that catalyst  
21  
22 aggregation---rather than Ostwald ripening---dominates the growth of metal particles.  
23  
24  
25  
26  
27  
28  
29  
30  
31  
32  
33  
34  
35  
36  
37  
38  
39  
40  
41  
42  
43  
44  
45  
46  
47  
48  
49  
50  
51  
52  
53  
54  
55  
56  
57  
58  
59  
60

## 1. Introduction

Controlling the size of a nano-material is critical for its application because the characteristic length of a material significantly affects its mechanical, thermal, chemical, and particularly electronic properties. This well known “size effect” has been intensively demonstrated in a variety of systems, including quantum dots, nanotubes, nanowires, nanoribbons/belts, etc.<sup>1-3</sup> For a single-walled carbon nanotube (SWNT), the diameter primarily determines the band-gap of a semi-conducting nanotube, and is therefore directly related to the performance of this material in electronics and optics applications.<sup>4-5</sup>

In 2004, we reported the first vertically aligned (VA-) SWNT array, which was synthesized by alcohol catalytic CVD (ACCVD)<sup>6</sup>. This method yields high-quality SWNTs with an average diameter of 2 nm. Since then, there have been considerable attempts to control the diameter of VA-SWNTs, among which the most successful work was reported in 2006 by Yamada et al., who managed to continuously tune the average diameter of the SWNTs from 2 to 5 nm.<sup>7</sup> More recently, Hart et al. demonstrated successful control over the diameter as well as the number of walls for single-walled and few-walled CNTs, being able to adjust the diameter from 5 to 100 nm.<sup>8</sup> However, extension of the range of VA-SWNT diameters to less than 2 nm remains a critical challenge. A diameter of 2 nm corresponds to roughly 0.4 eV of semiconductor SWNT band gap. Because the band gap is roughly inversely proportional to the diameter, SWNTs smaller than 2 nm in diameter are of interest for most electronics and optics applications.

The absence of sub-2 nm VA-SWNTs is mainly because the catalyst particles used for synthesizing VA-SWNTs are normally prepared by sputtering or evaporation.<sup>9-12</sup> In these conventional physical vapor deposition methods, it is an intrinsic challenge to reduce the size of the metal catalyst particles, which determine the size of the grown SWNT,<sup>13</sup> while maintaining

1  
2  
3 sufficient density necessary for vertical alignment. Here we report the ability to produce  
4 VA-SWNT arrays with a widely tunable average nanotube diameter. Our method can produce  
5 VA-SWNTs with an average diameter as small as 1.2 nm, which is about half of the minimum  
6 reported thus far in the literature. This small diameter is achieved using ACCVD and catalyst  
7 particles prepared by a wet process.<sup>6, 14</sup> Additionally, we performed a quantitative study on the  
8 diameter using a novel spectral analysis method, giving insights into the time-dependent SWNT  
9 formation process. Based on further investigations, a possible growth mechanism for  
10 small-diameter SWNT arrays is discussed.  
11  
12  
13  
14  
15  
16  
17  
18  
19  
20  
21  
22  
23

## 24 **2. Experimental**

25  
26 Vertically aligned SWNT arrays were synthesized on Co/Mo dip-coated quartz substrates  
27 using ethanol as the carbon source. The growth temperature, ethanol pressure, and concentration  
28 of the catalyst precursor were changed independently to investigate their effects on the diameter  
29 of obtained SWNTs. CVD duration was 5 min and the ethanol flow was 450 sccm in all cases.  
30 Additional details about the catalyst preparation and CVD procedure may be found in our  
31 previous reports.<sup>14-15</sup> The as-grown SWNT array was characterized by Scanning Electron  
32 Microscopy (SEM, Hitachi-5500), resonance Raman spectroscopy (488 and 633 nm excitation  
33 wavelengths), UV-vis-NIR absorbance spectroscopy (Shimadzu UV-3150), and Transmission  
34 Electron Microscopy (TEM, JEOL 2000EXII operated at 120 kV).  
35  
36  
37  
38  
39  
40  
41  
42  
43  
44  
45  
46  
47  
48  
49  
50

## 51 **3. Results**

### 52 **3.1 Characterization of VA-SWNT morphology and diameter**

53  
54  
55  
56  
57  
58  
59  
60

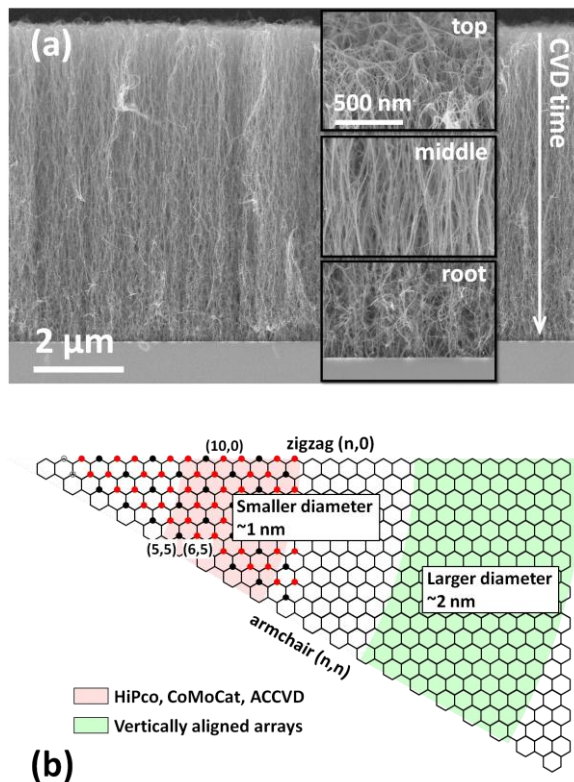


Figure 1. (a) A typical SEM image of a vertically aligned SWNT array grown on a quartz substrate shows the worsening alignment from top to bottom; insets are enlarged images of the top, middle, and root of the array. The scale bar applies to all three images. (b) A graphene lattice showing the chirality range of typical randomly aligned SWNTs (indicated in red) and vertically aligned SWNTs (indicated in green).

Figure 1a shows a typical SEM micrograph of a VA-SWNT array synthesized by ACCVD. The SWNTs grow perpendicular to the quartz substrate and form a self-standing forest-like array. The height of the array can be adjusted from sub-micrometer to hundreds of micrometers by changing CVD and catalyst preparation parameters. The average diameter of the SWNTs is approximately 2 nm using our standard procedure.<sup>16-17</sup> Although relatively small for vertically aligned SWNT arrays, 2 nm is considerably larger than non-aligned SWNTs synthesized by

1  
2  
3 powder-supported or floating catalyst methods (e.g. HiPco, CoMoCAT and zeolite-supported  
4  
5 ACCVD processes),<sup>18-19</sup> which yield SWNTs with diameters around 1 nm. The difference in  
6  
7 diameter range for VA-SWNTs and random SWNT aggregates is illustrated in Fig. 1b. We  
8  
9 acknowledge that large-diameter SWNTs (2 nm or larger) may be suitable or preferable in some  
10  
11 applications, (e.g., the diameter effect on device performance<sup>4</sup>), but small-diameter SWNTs (1  
12  
13 nm or less) possess considerable band-gaps, clearly setting them apart from graphene for  
14  
15 semiconductor electronics applications. The synthesis of small-diameter VA-SWNTs could  
16  
17 advance and extend the applications of this material.  
18  
19  
20  
21

22 We used optical absorbance as our primary method of characterizing diameter distribution,  
23  
24 with supplemental use of Raman scattering and TEM observations. It is important to summarize  
25  
26 the experimental methodologies being employed to characterize SWNT diameters because the  
27  
28 difficulty in diameter control lies not only in the synthesis protocols used but also in the  
29  
30 characterization methods and interpretation of data. Raman spectroscopy is perhaps the most  
31  
32 often used method because the frequency of the radial breathing mode (RBM) is directly  
33  
34 determined by the SWNT diameter.<sup>20</sup> However, Raman spectra contain information from a  
35  
36 limited number of SWNTs in the sample because excitation of the RBM is a resonance process  
37  
38 (unless a wide range of excitation energies are used), leaving the actual diameter distribution of  
39  
40 bulk SWNTs unclear. Furthermore, the strong dependence of Raman intensity on diameter and  
41  
42 chirality<sup>21</sup> hinders the use of this technique for the accurate estimation of diameter distribution.  
43  
44 Photoluminescence excitation spectroscopy (PLE) has more recently proved to be a powerful  
45  
46 technique for the unambiguous identification of SWNT chiralities.<sup>22</sup> However, the main  
47  
48 shortcoming of PLE, is that only isolated, small-diameter, semiconducting SWNTs can be  
49  
50 detected. Selectivity during sample preparation, a narrow detecting window, and  
51  
52  
53  
54  
55  
56  
57  
58  
59  
60

1  
2  
3 chirality-dependent quantum efficiencies also restrict the use of PLE for obtaining a statistically  
4 accurate result representative of the entire nanotube ensemble.<sup>23-24</sup> TEM and atomic force  
5 microscopy (AFM) in this sense are the most reliable methods, despite the complicated sample  
6 preparation and time-consuming measurement. Other strategies such as Rayleigh scattering<sup>25</sup> are  
7 applicable to only well isolated and suspended samples.  
8  
9  
10  
11  
12  
13  
14  
15  
16  
17

### 18 **3.2 Effects of CVD parameters**

19  
20 Figure 2 presents resonance Raman and optical absorbance spectra of vertically aligned  
21 SWNT films grown at various CVD temperatures and pressures using our standard catalyst  
22 recipe.<sup>14</sup> The resonance Raman spectra were taken directly from the top of the samples with 488  
23 nm laser excitation, and the optical absorbance spectra were obtained by titling the as-grown  
24 array 30 ° with respect to the Poynting vector of the incident light. Clear differences appear in the  
25 RBM region of the Raman spectra (red arrows in Fig. 2a), suggesting that SWNTs with smaller  
26 diameters are synthesized at elevated pressure and reduced temperature. The nearly identical  
27 positions of the E<sub>11</sub> and E<sub>22</sub> peaks<sup>26</sup> in the optical absorbance (Fig. 2b), however, imply the  
28 increase in the population of a minority of small-diameter SWNTs indicated by the Raman  
29 spectra is insufficient to alter the overall diameter distribution. This superficially contradictory  
30 result is because most of the strong RBM signals (145, 181, 244, 256 cm<sup>-1</sup>) are from a minority  
31 population of small-diameter SWNTs randomly suspended in the forest.<sup>27</sup> For example, from the  
32 Kataura plot<sup>28</sup> we know that RBM peaks at 244 and 256 cm<sup>-1</sup> correspond to (7,7) and (8,5)  
33 SWNTs with diameters of 0.96 and 0.90 nm, which are both far from the mean diameter of  
34 VA-SWNTs. In general, due to differences in resonance conditions as well as a stronger Raman  
35 response from small-diameter near-zigzag SWNTs,<sup>21</sup> small differences in sample populations  
36  
37  
38  
39  
40  
41  
42  
43  
44  
45  
46  
47  
48  
49  
50  
51  
52  
53  
54  
55  
56  
57  
58  
59  
60

can be greatly exaggerated in resonance Raman spectra. This is evidenced by a careful TEM characterization in which little difference in diameter distribution is observed (not shown).

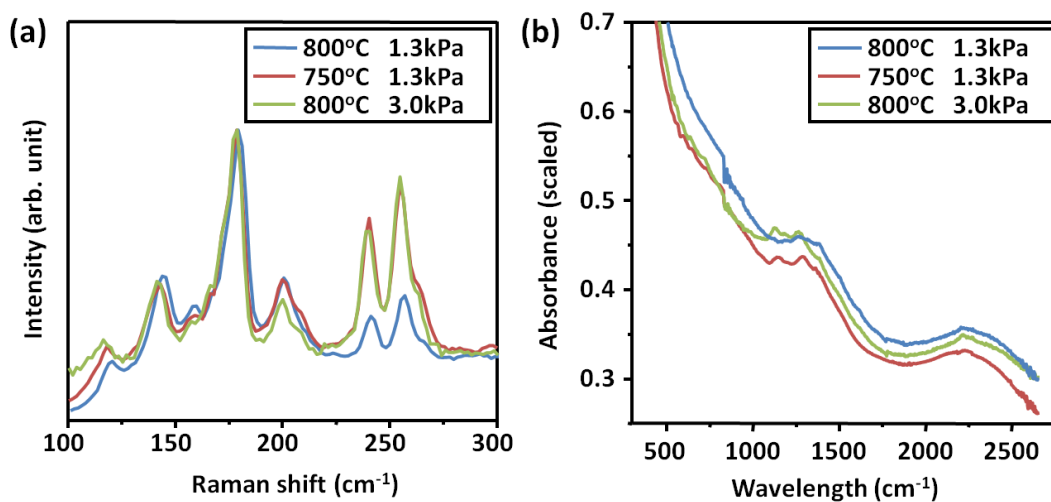


Figure 2. (a) Resonance Raman and (b) UV-vis-NIR optical absorbance spectra of aligned SWNTs grown at different temperatures and pressures clearly show different Raman RBM peak intensities but similar absorption peak positions. Excitation wavelength in (a) was 488 nm.

### 3.3 Effect of catalyst recipe

We find the influence of catalyst recipe on the diameters of produced SWNTs to be more significant than synthesis temperature or pressure. We have shown that the reduction of mean diameter can be achieved by modifying the reduction condition,<sup>29</sup> and by carefully adjusting the catalyst reduction condition to inhibit aggregation of catalysts we have obtained a mean diameter of 1.6 nm. Even though SWNTs with much smaller diameters can be obtained by exposing the catalyst to water vapor prior to CVD, vertically aligned morphology was lost due to less efficient growth from such catalysts.<sup>29</sup>



1  
2  
3 Since we use a bimetal Co-Mo catalyst in the present study, the effects of the two  
4 components were investigated independently. When the absolute amount of Co is decreased in  
5 the solution catalyst precursor, a clear blue-shift of the  $E_{11}$  and  $E_{22}$  peaks is seen in optical  
6 absorbance (Fig. 3a). Assuming the peak positions denote the mean diameter of the SWNTs  
7 inside the array, this suggests that the diameter reduces from 2 to 1.6 nm when the Co  
8 concentration is decreased by two orders of magnitude. This overall tendency is consistent with  
9 combinatorial experiments, in which the nominal thickness of Co and Mo were continuously  
10 changed.<sup>12</sup> Still, it is surprising that VA-SWNT morphology is obtained in this wide range of Co  
11 concentrations.  
12  
13  
14  
15  
16  
17  
18  
19  
20  
21  
22  
23

24 It seems qualitatively straightforward that a smaller amount of catalyst generates smaller  
25 catalyst particles, which produce thinner SWNTs.<sup>30</sup> It has also been proved that Co is the active  
26 site driving nanotube growth in our Co-Mo system.<sup>31</sup> However, unlike on porous catalyst  
27 supports such as zeolites<sup>32</sup> where nano-sized pores restrict the size of the catalyst, nanoparticles  
28 on a flat substrate always have a temperature-dependent minimum size limit determined by the  
29 energy of the system. Furthermore, small particles can easily migrate and aggregate at elevated  
30 temperature. One common strategy to inhibit this aggregation is to introduce a secondary species,  
31 such as molybdenum<sup>12, 31</sup> or alumina<sup>9</sup>. Therefore, the role of Mo in our Co-Mo system is also  
32 studied independently.  
33  
34  
35  
36  
37  
38  
39  
40  
41  
42  
43  
44  
45  
46  
47  
48  
49  
50  
51  
52  
53  
54  
55  
56  
57  
58  
59  
60

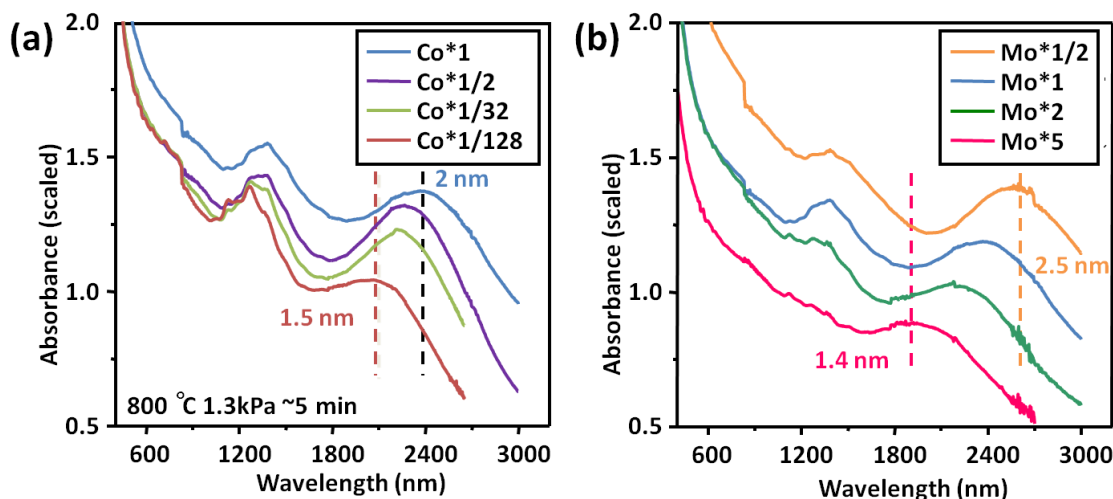
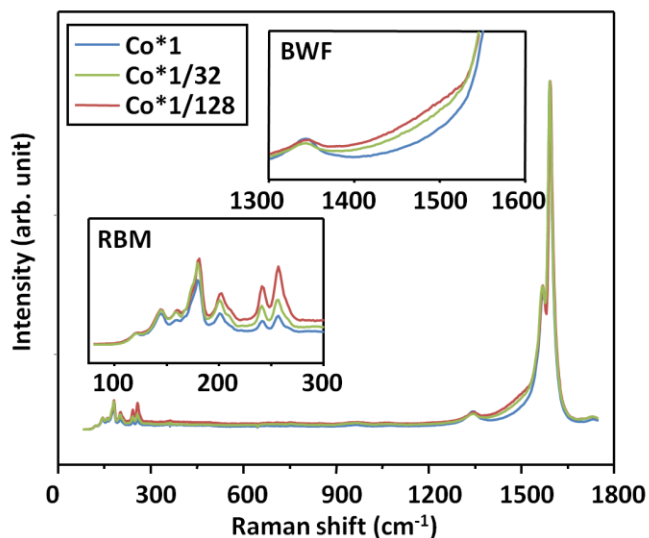


Figure 3. (a) UV-vis-NIR optical absorbance spectra of aligned SWNTs synthesized using different catalyst recipes. The concentration of the catalyst solution is normalized by a standard value of 0.01wt% for each of the metal species in cobalt acetate and molybdenum acetate.

Figure 3b shows optical absorbance spectra of VA-SWNTs grown using different Mo concentrations while keeping the Co concentration constant. The  $E_{11}$  and  $E_{22}$  peaks of the produced SWNTs exhibit more significant shifts than in the reduced Co case, indicating the average diameter changed from 2.5 nm to 1.4 nm. This diameter reduction was achieved by increasing the Mo concentration by only ten times, yet is much more significant than the reduction obtained by reducing the Co concentration by a factor of more than 100. This agrees well with the hypothesis that Mo forms an oxide that strongly interacts with Co, thereby reducing the mobility of Co nanoparticles at high temperatures.<sup>12, 31</sup>

Two significant changes can be observed in resonant Raman spectra (Figure 4) from the reduced-concentration-Co recipe, and are consistent with the above absorption results. First, higher-frequency peaks in the RBM range are enhanced in the sample grown using the least amount of Co. This indicates an increased population of small-diameter SWNTs. Secondly,

1  
2  
3 decreasing the amount of Co also leads to an emergence of a more intense Breit-Wigner-Fano  
4 (BWF) feature in the G-band region, also indicating an increased contribution of small-diameter  
5 (BWF) feature in the G-band region, also indicating an increased contribution of small-diameter  
6 metallic nanotubes such as (7,7) and (8,5). However, the relatively weak BWF signal from our  
7 VA-SWNTs for a wide range of diameters and different excitation energies (not shown) cannot  
8 be straightforwardly understood. Because a considerable contribution to the G-band from  
9 majority larger diameter and vertically aligned nanotubes is apparent from polarized Raman  
10 measurements,<sup>27</sup> silence of metallic nanotube features may imply that the percentage of  
11 semiconductor nanotubes is high. Similar results were obtained for the increased-Mo case. As  
12 stated above, such changes in the Raman spectra are not sufficient evidence for overall diameter  
13 modulation, and agreement with absorbance spectra is necessary.  
14  
15  
16  
17  
18  
19  
20  
21  
22  
23  
24  
25  
26  
27  
28  
29



49 Figure 4. Resonance Raman spectra of vertically aligned SWNTs obtained from ACCVD with  
50 reduced Co amount on quartz substrates. Indication of the existence of smaller diameter SWNTs  
51 is consistent with optical absorbance spectra. Excitation wavelength was 488 nm.  
52  
53  
54  
55  
56  
57  
58  
59  
60

1  
2  
3 High-resolution TEM (HR-TEM) characterization was performed on samples obtained in the  
4 above-mentioned experiments. For consistency, we chose the upper portions of the arrays for all  
5 TEM observations. Micrographs of a typical SWNT array and a small-diameter array are shown  
6 in Figs 5a and 5b, respectively. We measured the diameters of approximately 400 SWNTs and  
7 present the statistics in Figure 5c. The histograms show three representative samples, with  
8 average diameters of 2.0, 1.6 and 1.2 nm. Although time-consuming, this TEM measurement  
9 unambiguously reveals the diameter distribution was successfully modulated over a broad range.  
10 Furthermore, for the  $d_{\text{avg}} = 1.2$  nm sample, all SWNTs in the array were found to be thinner than  
11 2 nm, which may be critically important for some applications. We note that the mean diameter  
12 estimated from optical absorbance spectra is slightly larger than the value obtained from TEM  
13 observations (e.g., 1.4 nm vs. 1.2 nm). The reason for this is explained in the following section.  
14 It is also worth noting that although SWNTs with mean diameters of less than 1.2 nm may be  
15 obtained by further reducing the Co or increasing the Mo concentration, the catalyst activity  
16 decreases dramatically and the vertical alignment is therefore lost. Very recently, we also  
17 reported the growth of nitrogen-doped VA-SWNTs with a mean diameter of 0.7 nm by using  
18 mixed ethanol/acetonitrile carbon source.<sup>33</sup> However, for un-doped VA-SWNTs, further  
19 reducing the diameter while maintaining vertical alignment still presents a challenge.  
20  
21  
22  
23  
24  
25  
26  
27  
28  
29  
30  
31  
32  
33  
34  
35  
36  
37  
38  
39  
40  
41  
42  
43  
44  
45  
46  
47  
48  
49  
50  
51  
52  
53  
54  
55  
56  
57  
58  
59  
60

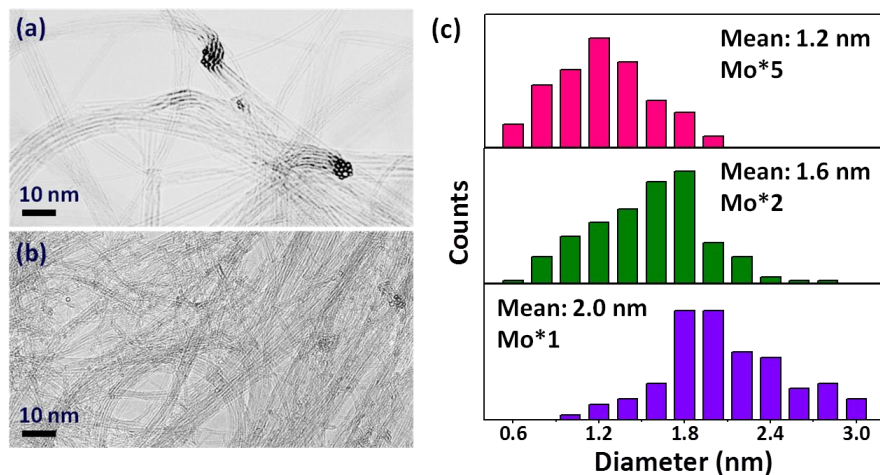


Figure 5. (a),(b) Representative TEM images and (c) diameter histograms of vertically aligned SWNTs synthesized using different catalyst recipes.

### 3.4 Quantitative measurement of diameter along SWNT array

Vertically aligned SWNTs normally obey a root growth mechanism,<sup>34-38</sup> and all SWNTs grow in generally the same direction. The resulting alignment enables easy access to regions in the array where SWNTs formed at different times during synthesis, thus study of the time-dependent growth process becomes possible. For example, in the SEM image shown in Fig 1a, it appears that the upper portion of the array (grown earlier) is better aligned than the root (grown later). The bundle size also appears to decrease with CVD time. Resonance Raman spectra taken from different points along the cross-section of the array C (Fig. 6a) also show a marked difference. Note that the anomalous effect of suspended nanotubes<sup>27</sup> is less pronounced for excitation with a 633 nm laser.<sup>39</sup> Low-energy RBM peaks (i.e., from large-diameter SWNTs) are enhanced in spectra obtained near the root of the array.

1  
2  
3 For a more quantitative characterization, we synthesized three VA-SWNT arrays (called A, B,  
4 and C for convenience) by changing only the CVD time; other parameters were kept strictly  
5 identical. The dependence of film thickness on growth time (depicted by a growth curve<sup>40</sup>) is  
6 shown for each array in Fig. 6b. These three growth curves suggest that all three samples  
7 exhibited almost exactly the same growth behavior, having nearly identical growth rates and  
8 catalyst deactivation times. Optical absorbance spectra corresponding to each of these arrays are  
9 shown in Figure 6c, and little difference is seen in the E<sub>11</sub> and E<sub>22</sub> peak positions.

10  
11  
12  
13  
14  
15  
16  
17  
18  
19  
20 Assuming the only difference in these SWNT arrays is their height, we can consider the arrays  
21 are nearly approximated as combinations of the others. In this approach, array A is simply an  
22 array with height 3 μm, and is represented by the green box in Fig. 6b. Array B (height = 6 μm,  
23 purple box in Fig. 6b), may be considered as two 3-μm arrays stacked on top of each other. The  
24 upper 3-μm array should be identical to array A, so subtracting spectrum A from the spectrum of  
25 array B should yield the absorbance contribution from the bottom half of array B (blue box in  
26 Fig. 6b). Similarly, subtracting spectrum B from that for C gives the net absorbance of the root  
27 part of array C (red box in Fig. 6b). Using this strategy, the absorbance of array C (an 8-μm  
28 SWNT array) can be decomposed into three spectra, spectrum A (top), spectrum B-A (middle),  
29 and spectrum C-B (root). The spectra decomposed in this manner are shown in Figure 6d. The  
30 peak positions are clearly different, indicating that the SWNT diameters are *not* uniform along  
31 the array, and the SWNTs synthesized last (near the root) have larger diameters than those which  
32 form first (at the top). This gradual increase of the SWNT diameter with growth time was  
33 observed before by Hasegawa et al.<sup>41</sup> but generally difficult to characterize by conventional  
34 approaches. This “sliced” optical absorbance method offers a quantitative evaluation and  
35 confirms the diameter change is approximately 20% in the present case.

36  
37  
38  
39  
40  
41  
42  
43  
44  
45  
46  
47  
48  
49  
50  
51  
52  
53  
54  
55  
56  
57  
58  
59  
60

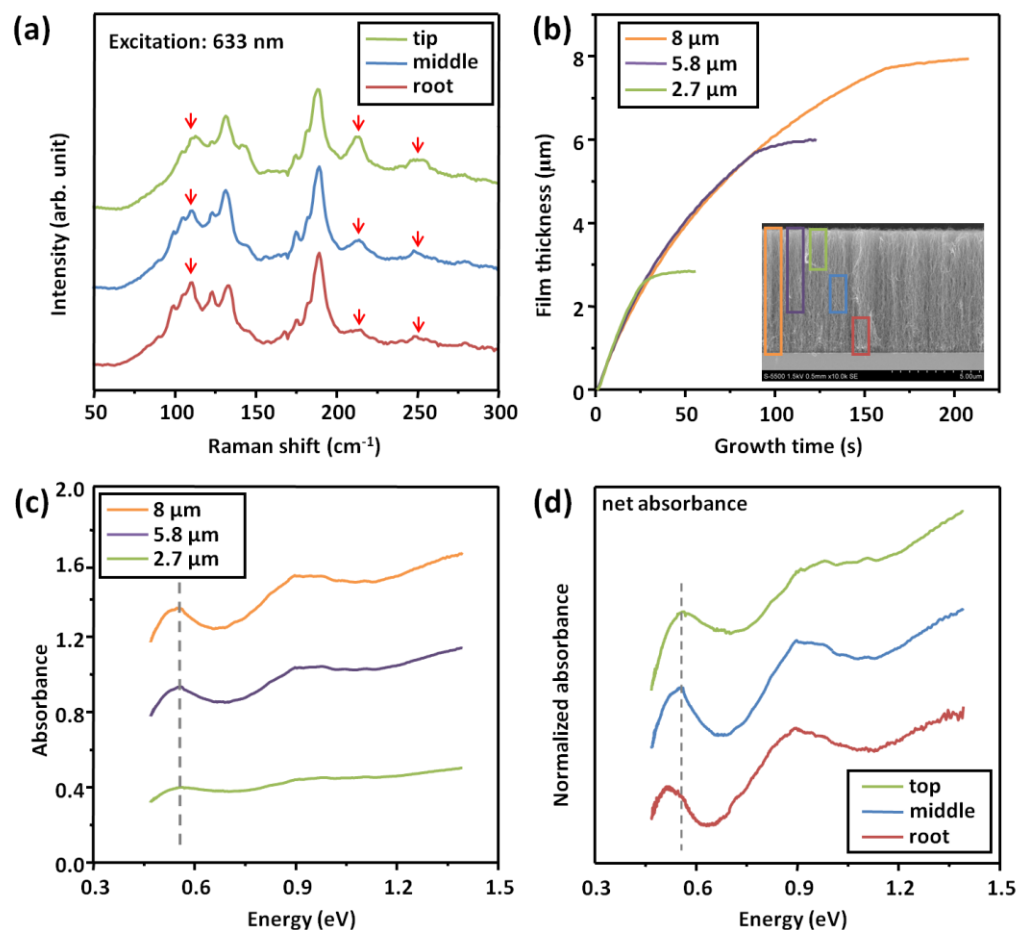


Figure 6. (a) Raman spectra obtained from the top, middle, and root of a cross-section of a typical aligned SWNT array showing that the diameter of SWNTs at the root seems to be larger than at the top. Excitation wavelength was 633 nm; (b) growth curves of three arrays grown under strictly identical CVD conditions but for different times. Inset shows the morphology of the VA-SWNTs; (c) optical absorbance of the three arrays; (d) net/absolute absorbance of the different parts of the 8  $\mu\text{m}$  array obtained by subtracting the data in (c). Shifts in peak positions quantitatively show the diameter change occurring during synthesis.

1  
2  
3 The spectra shown in Fig. 6 also help to understand why the average diameter obtained from  
4 TEM is slightly smaller than suggested by optical absorbance. The difference between diameter  
5 estimates based on optical absorbance and HR-TEM measurements shown in Fig. 5 is likely  
6 because the former averages the entire array, whereas the latter is only representative of a local  
7 region that may not necessarily be representative of the entire array. Nevertheless, the results  
8 shown in Fig. 5 indicate VA-SWNTs with diameters as small as 1.2 nm can be obtained.  
9  
10 Previous VA-SWNTs grown on physical vapor deposited catalyst usually have diameters larger  
11 than 2 nm.  
12  
13  
14  
15  
16  
17  
18  
19  
20  
21  
22  
23

### 24 **3.5 Mechanism for diameter change: ripening or aggregation**

25  
26 Since the SWNT diameter is essentially determined by the size of the catalyst particle,<sup>13</sup> the  
27 observed diameter change reveals the behavior of the catalyst on a flat substrate. At high  
28 temperature there are two competing mechanisms that can lead to particle growth. At CVD  
29 temperatures, the catalyst particles are mobile on the substrate and may collide with each other,  
30 forming a larger particle. Less mobile particles can also grow via Ostwald ripening.<sup>41-42</sup> The  
31 main difference between these two processes is that in Ostwald ripening small particles gradually  
32 lose atoms to larger particles, causing the larger particles to grow and smaller ones to shrink.  
33 This would cause the distribution of an ensemble of particles to shift from Gaussian to bimodal.  
34 Since our sliced absorbance spectra in Fig. 6d reveal a general shift in one direction (no split in  
35 the small diameter range), it appears that catalyst aggregation---rather than Ostwald  
36 ripening---dominates catalyst behavior during the growth of our SWNTs.<sup>43</sup>  
37  
38  
39  
40  
41  
42  
43  
44  
45  
46  
47  
48  
49  
50  
51  
52

53 To confirm this speculation we investigated the catalyst morphology by TEM after different  
54 CVD times (Supporting material). To make the observation less challenging we intentionally  
55  
56  
57  
58  
59  
60



1  
2  
3 used a high-concentration catalyst solution to form slightly larger catalyst particles. TEM  
4 micrographs and a statistical histogram showing catalyst sizes (Fig. S1) reveal that in the early  
5 stage of the CVD process all particles are below 3 nm, whereas after 10 min all catalyst sizes  
6 increase to approximately 3.5 nm. No noticeable enhancement of small diameter particles was  
7 observed. These findings indicate that Ostwald ripening is not the primary mechanism behind  
8 catalyst growth in this process.  
9  
10  
11  
12  
13  
14  
15  
16  
17  
18  
19

#### 20 **4. Summary**

21 We present a comprehensive study on the diameter modulation of vertically aligned SWNT  
22 arrays, and show that the catalyst recipe has a much more significant impact on mean diameter  
23 than either CVD temperature or pressure. By changing both the relative and absolute amounts of  
24 Co and Mo in a binary catalyst system, we were able to tune the average SWNT diameter  
25 between 1.2 and 2.5 nm, as determined by optical absorbance, resonance Raman spectroscopy,  
26 and HR-TEM. For the mean diameter of 1.2 nm, all the SWNTs were found to be thinner than 2  
27 nm. Due to their nearly doubled band gap and improved structural stiffness, such small-diameter  
28 VA-SWNTs may be desirable for optical and electronic applications. We also propose a method  
29 by which optical absorbance spectra can be decomposed to reveal contributions from different  
30 parts of a SWNT array. By this method, we reveal a 20% increase in SWNT diameter during  
31 CVD synthesis, which we attribute to catalyst aggregation rather than Ostwald ripening. These  
32 insights into the growth mechanism may help researchers to further control the synthesis of this  
33 material.  
34  
35  
36  
37  
38  
39  
40  
41  
42  
43  
44  
45  
46  
47  
48  
49  
50  
51  
52  
53  
54  
55  
56  
57  
58  
59  
60

## Acknowledgment

Part of this work was financially supported by Grant-in-Aid for Scientific Research (22226006 , 19054003, 23760179 and 23760180), JSPS Core-to-Core Program, the "Global Center for Excellence for Mechanical Systems Innovation" program at the University of Tokyo, National Science Foundation of China (51002190), and Guangdong Provincial Natural Science Foundation of China.

**Figure captions**

1  
2  
3  
4  
5  
6  
7  
8  
9  
10  
11  
12  
13  
14  
15  
16  
17  
18  
19  
20  
21  
22  
23  
24  
25  
26  
27  
28  
29  
30  
31  
32  
33  
34  
35  
36  
37  
38  
39  
40  
41  
42  
43  
44  
45  
46  
47  
48  
49  
50  
51  
52  
53  
54  
55  
56  
57  
58  
59  
60

Figure 1. (a) A typical SEM image of a vertically aligned SWNT array grown on a quartz substrate shows the worsening alignment; insets are enlarged images of the top, middle, and root of the array. The scale bar applies to all three images. (b) A graphene lattice showing the chirality range of common randomly aligned SWNTs (indicated in red) and vertically aligned SWNTs (indicated in green).

Figure 2. (a) Resonance Raman and (b) UV-vis-NIR optical absorbance spectra of aligned SWNTs grown at different temperatures and pressures clearly show different Raman RBM peak intensities but similar absorption peak positions. Excitation wavelength in (a) was 488 nm.

Figure 3. (a) UV-vis-NIR optical absorbance spectra of aligned SWNTs synthesized using different catalyst recipes. The concentration of the catalyst solution is normalized by a standard value of 0.01wt% for each of the metal species in cobalt acetate and molybdenum acetate.

Figure 4. Resonance Raman spectra of vertically aligned SWNTs obtained from ACCVD with reduced Co amount on quartz substrates. Indication of the existence of smaller diameter SWNTs is consistent with optical absorbance data. Excitation wavelength was 488 nm.

1  
2  
3  
4 Figure 5. (a),(b) Representative TEM images and (c) diameter histograms of vertically aligned  
5  
6  
7 SWNTs synthesized using different catalyst recipes.  
8  
9

10  
11  
12 Figure 6. (a) Raman spectra obtained from the top, middle, and root of a cross-section of a  
13  
14 typical aligned SWNT array showing that the diameter of SWNTs at root seems to be larger than  
15  
16 at the top. Excitation wavelength was 633 nm; (b) growth curves of three arrays grown under  
17  
18 strictly identical CVD conditions but for different times. Inset shows the morphology of the  
19  
20 VA-SWNTs; (c) optical absorbance of the three arrays; (d) net/absolute absorbance of the  
21  
22 different parts of the 8  $\mu\text{m}$  array obtained by subtracting the data in (c). Shifts in peak positions  
23  
24  
25 quantitatively show the diameter change occurring during synthesis.  
26  
27  
28  
29  
30  
31  
32  
33  
34  
35  
36  
37  
38  
39  
40  
41  
42  
43  
44  
45  
46  
47  
48  
49  
50  
51  
52  
53  
54  
55  
56  
57  
58  
59  
60

## References

1. Burda, C.; Chen, X. B.; Narayanan, R.; El-Sayed, M. A., Chemistry and properties of nanocrystals of different shapes. *Chem Rev* **2005**, *105* (4), 1025-1102.
2. Hu, J. T.; Odom, T. W.; Lieber, C. M., Chemistry and physics in one dimension: Synthesis and properties of nanowires and nanotubes. *Accounts Chem Res* **1999**, *32* (5), 435-445.
3. Jiao, L. Y.; Zhang, L.; Wang, X. R.; Diankov, G.; Dai, H. J., Narrow graphene nanoribbons from carbon nanotubes. *Nature* **2009**, *458* (7240), 877-880.
4. Asada, Y.; Nihey, F.; Ohmori, S.; Shinohara, H.; Saito, T., Diameter-Dependent Performance of Single-Walled Carbon Nanotube Thin-Film Transistors. *Adv Mater* **2011**, *23* (40), 4631-4635.
5. Kataura, H.; Kumazawa, Y.; Maniwa, Y.; Umez, I.; Suzuki, S.; Ohtsuka, Y.; Achiba, Y., Optical properties of single-wall carbon nanotubes. *Synthetic Met* **1999**, *103* (1-3), 2555-2558.
6. Maruyama, S.; Kojima, R.; Miyauchi, Y.; Chiashi, S.; Kohno, M., Low-temperature synthesis of high-purity single-walled carbon nanotubes from alcohol. *Chem Phys Lett* **2002**, *360* (3-4), 229-234.
7. Yamada, T.; Namai, T.; Hata, K.; Futaba, D. N.; Mizuno, K.; Fan, J.; Yudasaka, M.; Yumura, M.; Iijima, S., Size-selective growth of double-walled carbon nanotube forests from engineered iron catalysts. *Nat Nanotechnol* **2006**, *1* (2), 131-136.
8. Nessim, G. D.; Hart, A. J.; Kim, J. S.; Acquaviva, D.; Oh, J. H.; Morgan, C. D.; Seita, M.; Leib, J. S.; Thompson, C. V., Tuning of Vertically-Aligned Carbon Nanotube Diameter and Areal Density through Catalyst Pre-Treatment. *Nano Lett* **2008**, *8* (11), 3587-3593.
9. Hata, K.; Futaba, D. N.; Mizuno, K.; Namai, T.; Yumura, M.; Iijima, S., Water-assisted highly efficient synthesis of impurity-free single-walled carbon nanotubes. *Science* **2004**, *306* (5700), 1362-1364.
10. Zhang, G. Y.; Mann, D.; Zhang, L.; Javey, A.; Li, Y. M.; Yenilmez, E.; Wang, Q.; McVittie, J. P.; Nishi, Y.; Gibbons, J.; Dai, H. J., Ultra-high-yield growth of vertical single-walled carbon nanotubes: Hidden roles of hydrogen and oxygen. *P Natl Acad Sci USA* **2005**, *102* (45), 16141-16145.
11. Zhong, G. F.; Iwasaki, T.; Honda, K.; Furukawa, Y.; Ohdomari, I.; Kawarada, H., Low temperature synthesis of extremely dense, and vertically aligned single-walled carbon nanotubes. *Jpn J Appl Phys I* **2005**, *44* (4A), 1558-1561.
12. Sugime, H.; Noda, S.; Maruyama, S.; Yamaguchi, Y., Multiple "optimum" conditions for Co-Mo catalyzed growth of vertically aligned single-walled carbon nanotube forests. *Carbon* **2009**, *47* (1), 234-241.
13. Homma, Y.; Kobayashi, Y.; Ogino, T.; Takagi, D.; Ito, R.; Jung, Y. J.; Ajayan, P. M., Role of transition metal catalysts in single-walled carbon nanotube growth in chemical vapor deposition. *J Phys Chem B* **2003**, *107* (44), 12161-12164.
14. Murakami, Y.; Chiashi, S.; Miyauchi, Y.; Hu, M. H.; Ogura, M.; Okubo, T.; Maruyama, S., Growth of vertically aligned single-walled carbon nanotube films on quartz substrates and their optical anisotropy. *Chem Phys Lett* **2004**, *385* (3-4), 298-303.
15. Xiang, R.; Wu, T. Z.; Einarsson, E.; Suzuki, Y.; Murakami, Y.; Shiomi, J.; Maruyama, S., High-Precision Selective Deposition of Catalyst for Facile Localized Growth of Single-Walled Carbon Nanotubes. *J Am Chem Soc* **2009**, *131* (30), 10344-10345.

16. Murakami, Y.; Einarsson, E.; Edamura, T.; Maruyama, S., Polarization dependent optical absorption properties of single-walled carbon nanotubes and methodology for the evaluation of their morphology. *Carbon* **2005**, *43* (13), 2664-2676.
17. Xiang, R.; Yang, Z.; Zhang, Q.; Luo, G. H.; Qian, W. Z.; Wei, F.; Kadowaki, M.; Einarsson, E.; Maruyama, S., Growth deceleration of vertically aligned carbon nanotube arrays: Catalyst deactivation or feedstock diffusion controlled? *J Phys Chem C* **2008**, *112* (13), 4892-4896.
18. Nikolaev, P.; Bronikowski, M. J.; Bradley, R. K.; Rohmund, F.; Colbert, D. T.; Smith, K. A.; Smalley, R. E., Gas-phase catalytic growth of single-walled carbon nanotubes from carbon monoxide. *Chem Phys Lett* **1999**, *313* (1-2), 91-97.
19. Bachilo, S. M.; Balzano, L.; Herrera, J. E.; Pompeo, F.; Resasco, D. E.; Weisman, R. B., Narrow (n,m)-distribution of single-walled carbon nanotubes grown using a solid supported catalyst. *J Am Chem Soc* **2003**, *125* (37), 11186-11187.
20. Jorio, A.; Saito, R.; Hafner, J. H.; Lieber, C. M.; Hunter, M.; McClure, T.; Dresselhaus, G.; Dresselhaus, M. S., Structural (n, m) determination of isolated single-wall carbon nanotubes by resonant Raman scattering. *Phys Rev Lett* **2001**, *86* (6), 1118-1121.
21. Sato, K.; Saito, R.; Nugraha, A. R. T.; Maruyama, S., Excitonic effects on radial breathing mode intensity of single wall carbon nanotubes. *Chem Phys Lett* **2010**, *497* (1-3), 94-98.
22. O'Connell, M. J.; Bachilo, S. M.; Huffman, C. B.; Moore, V. C.; Strano, M. S.; Haroz, E. H.; Rialon, K. L.; Boul, P. J.; Noon, W. H.; Kittrell, C.; Ma, J. P.; Hauge, R. H.; Weisman, R. B.; Smalley, R. E., Band gap fluorescence from individual single-walled carbon nanotubes. *Science* **2002**, *297* (5581), 593-596.
23. Oyama, Y.; Saito, R.; Sato, K.; Jiang, J.; Samsonidze, G. G.; Gruneis, A.; Miyauchi, Y.; Maruyama, S.; Jorio, A.; Dresselhaus, G.; Dresselhaus, M. S., Photoluminescence intensity of single-wall carbon nanotubes. *Carbon* **2006**, *44* (5), 873-879.
24. Tsyboulski, D. A.; Rocha, J. D. R.; Bachilo, S. M.; Cagnet, L.; Weisman, R. B., Structure-dependent fluorescence efficiencies of individual single-walled carbon nanotubes. *Nano Lett* **2007**, *7* (10), 3080-3085.
25. Sfeir, M. Y.; Wang, F.; Huang, L. M.; Chuang, C. C.; Hone, J.; O'Brien, S. P.; Heinz, T. F.; Brus, L. E., Probing electronic transitions in individual carbon nanotubes by Rayleigh scattering. *Science* **2004**, *306* (5701), 1540-1543.
26. Tian, Y.; Nasibulin, A. G.; Aitchison, B.; Nikitin, T.; von Pfaer, J.; Jiang, H.; Zhu, Z.; Khriachtchev, L.; Brown, D. P.; Kauppinen, E. I., Controlled Synthesis of Single-Walled Carbon Nanotubes in an Aerosol Reactor. *J Phys Chem C* **2011**, *115* (15), 7309-7318.
27. Zhang, Z. Y.; Einarsson, E.; Murakami, Y.; Miyauchi, Y.; Maruyama, S., Polarization dependence of radial breathing mode peaks in resonant Raman spectra of vertically aligned single-walled carbon nanotubes. *Phys Rev B* **2010**, *81* (16).
28. Araujo, P. T.; Doorn, S. K.; Kilina, S.; Tretiak, S.; Einarsson, E.; Maruyama, S.; Chacham, H.; Pimenta, M. A.; Jorio, A., Third and fourth optical transitions in semiconducting carbon nanotubes. *Phys Rev Lett* **2007**, *98* (6).
29. Thurakitseree, T.; Einarsson, E.; Xiang, R.; Zhao, P.; Aikawa, S.; Chiashi, S.; Shiomi, J.; Maruyama, S., Diameter Controlled Chemical Vapor Deposition Synthesis of Single-Walled Carbon Nanotubes. *J Nanosci Nanotechnol* **2012**, *12* (1), 370-376.
30. Helveg, S.; Lopez-Cartes, C.; Sehested, J.; Hansen, P. L.; Clausen, B. S.; Rostrup-Nielsen, J. R.; Abild-Pedersen, F.; Nørskov, J. K., Atomic-scale imaging of carbon nanofibre growth. *Nature* **2004**, *427* (6973), 426-429.

- 1
  - 2
  - 3
  - 4
  - 5
  - 6
  - 7
  - 8
  - 9
  - 10
  - 11
  - 12
  - 13
  - 14
  - 15
  - 16
  - 17
  - 18
  - 19
  - 20
  - 21
  - 22
  - 23
  - 24
  - 25
  - 26
  - 27
  - 28
  - 29
  - 30
  - 31
  - 32
  - 33
  - 34
  - 35
  - 36
  - 37
  - 38
  - 39
  - 40
  - 41
  - 42
  - 43
  - 44
  - 45
  - 46
  - 47
  - 48
  - 49
  - 50
  - 51
  - 52
  - 53
  - 54
  - 55
  - 56
  - 57
  - 58
  - 59
  - 60
31. Hu, M. H.; Murakami, Y.; Ogura, M.; Maruyama, S.; Okubo, T., Morphology and chemical state of Co-Mo catalysts for growth of single-walled carbon nanotubes vertically aligned on quartz substrates. *J Catal* **2004**, *225* (1), 230-239.
32. Okamoto, A.; Shinohara, H., Control of diameter distribution of single-walled carbon nanotubes using the zeolite-CCVD method at atmospheric pressure. *Carbon* **2005**, *43* (2), 431-436.
33. Thurakitseree, T.; Kramberger, C.; Zhao, P.; Aikawa, S.; Harish, S.; Chiashi, S.; Einarsson, E.; Maruyama, S., Diameter-controlled and nitrogen-doped vertically aligned single-walled carbon nanotubes. *Carbon* **2012**, *50* (7), 2635-2640.
34. Liu, L.; Fan, S. S., Isotope labeling of carbon nanotubes and a formation of C-12-C-13 nanotube junctions. *J Am Chem Soc* **2001**, *123* (46), 11502-11503.
35. Li, X.; Cao, A. Y.; Jung, Y. J.; Vjatai, R.; Ajayan, P. M., Bottom-Up Growth of Carbon Nanotube Multilayers: Unprecedented Growth. *Nano Lett* **2005**, *5* (10), 1997-2000.
36. Xiang, R.; Luo, G. H.; Qian, W. Z.; Zhang, Q.; Wang, Y.; Wei, F.; Li, Q.; Cao, A. Y., Encapsulation, compensation, and substitution of catalyst particles during continuous growth of carbon nanotubes. *Adv Mater* **2007**, *19* (17), 2360-2360.
37. Xiang, R.; Zhang, Z.; Ogura, K.; Okawa, J.; Einarsson, E.; Miyauchi, Y.; Shiomi, J.; Maruyama, S., Vertically Aligned <sup>13</sup>C Single-Walled Carbon Nanotubes from No-flow Alcohol Chemical Vapor Deposition and their Root Growth Mechanism. *Jpn J Appl Phys* **2008**, *47* (4), 1971-1974.
38. Iwasaki, T.; Zhong, G. F.; Aikawa, T.; Yoshida, T.; Kawarada, H., Direct evidence for root growth of vertically aligned single-walled carbon nanotubes by microwave plasma chemical vapor deposition. *J Phys Chem B* **2005**, *109* (42), 19556-19559.
39. Murakami, Y.; Chiashi, S.; Einarsson, E.; Maruyama, S., Polarization dependence of resonant Raman scattering from vertically aligned single-walled carbon nanotube films. *Phys Rev B* **2005**, *71* (8).
40. Einarsson, E.; Murakami, Y.; Kadowaki, M.; Maruyama, S., Growth dynamics of vertically aligned single-walled carbon nanotubes from in situ measurements. *Carbon* **2008**, *46* (6), 923-930.
41. Hasegawa, K.; Noda, S., Millimeter-Tall Single-Walled Carbon Nanotubes Rapidly Grown with and without Water. *ACS Nano* **2011**, *5* (2), 975-984.
42. Hasegawa, K.; Noda, S., Moderating carbon supply and suppressing Ostwald ripening of catalyst particles to produce 4.5-mm-tall single-walled carbon nanotube forests. *Carbon* **2011**, *49* (13), 4497-4504.
43. Sakurai, S.; Nishino, H.; Futaba, D.; Yasuda, S.; Yamada, T.; Maigne, A.; Matsuo, Y.; Nakamura, E.; Yumura, M.; Hata, K., Role of Subsurface Diffusion and Ostwald Ripening in Catalyst Formation for Single-Walled Carbon Nanotube Forest Growth. *J Am Chem Soc* **2012**, *134*, 2148-2153.

## Supporting Information Available:

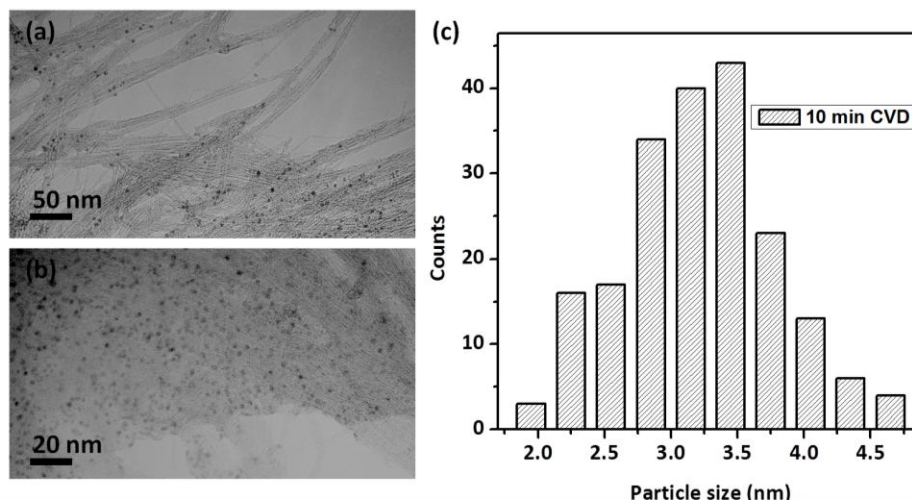


Figure S1. (a),(b) Typical TEM images and (c) diameter distribution histogram of the catalyst particles at the root of an SWNT array after 10 min CVD.



Table of content graphic

